Solar Phys (2007) 245: 251–262
DOI 10.1007/s11207-007-9054-y

Calculating and Testing Nonlinear Force-Free Fields

M.S. Wheatland

Received: 20 July 2007 / Accepted: 19 September 2007 / Published online: 16 October 2007

Abstract Improvements to an existing method for calculating nonlinear force-free magnetic fields (Wheatland, *Solar Phys.* **238**, 29, 2006) are described. In particular a solution of the 3-D Poisson equation using 2-D Fourier transforms is presented. The improved nonlinear force-free method is demonstrated in application to linear force-free test cases with localized nonzero values of the normal component of the field in the boundary. These fields provide suitable test cases for nonlinear force-free calculations because the boundary conditions involve localized nonzero values of the normal components of the field and of the current density, and because (being linear force-free fields) they have more direct numerical solutions. Despite their simplicity, fields of this kind have not been recognized as test cases for nonlinear methods before. The examples illustrate the treatment of the boundary conditions on current in the nonlinear force-free method, and in particular the limitations imposed by field lines that connect outside of the boundary region.

Keywords Active regions: magnetic fields · Active regions: models · Corona: models · Magnetic fields: corona · Magnetic fields: models

1. Introduction

Coronal magnetic fields govern solar activity, so there is considerable interest in their accurate modeling. The most detailed determinations of magnetic field values on the Sun come from polarization measurements of spectral lines in the low solar atmosphere. In principle photospheric and chromospheric vector magnetic field values derived from these measurements may be used as boundary values for calculating the overlying coronal field.

A popular approach involves assuming the coronal magnetic field **B** is force-free, that is, has zero Lorentz force (*e.g.*, McClymont, Jiao, and Mikic, 1997; Amari *et al.*, 1997; Neukirch, 2005). The problem then consists of solving the nonlinear force-free equations

M.S. Wheatland (✉)
School of Physics, University of Sydney, Sydney, Australia
e-mail: m.wheatland@physics.usyd.edu.au

$(\nabla \times \mathbf{B}) \times \mathbf{B} = 0$ together with $\nabla \cdot \mathbf{B} = 0$ subject to suitable boundary conditions derived from the data. An alternative statement of the equations is

$$\nabla \times \mathbf{B} = \alpha \mathbf{B} \tag{1}$$

and

$$\mathbf{B} \cdot \nabla \alpha = 0, \tag{2}$$

where α is the force-free parameter. In this form the appropriate boundary conditions are the specification of B_n, the normal component of $\mathbf{B}$ in the boundary, together with α over one polarity of B_n (one sign of B_n). The values of α over one polarity together with B_n specify the normal component of the current density $J_\mathrm{n} = \alpha B_\mathrm{n}/\mu_0$ over the polarity. Typically the curvature of the Sun is neglected and the problem is considered in the half space $z > 0$, with $z = 0$ as the boundary.

There are many difficulties with the nonlinear force-free approach to coronal field modeling. Key difficulties include uncertainties in the inversion of spectropolarimetric measurements to yield magnetic field values, the problem of the 180-degree ambiguity in the azimuthal angle of the field component transverse to the line of sight (*e.g.*, Metcalf *et al.*, 2006), the intrinsic difficulty of solving the coupled nonlinear partial differential equations, and the inconsistency of the boundary data with the force-free assumption (*e.g.*, Metcalf *et al.*, 1995, 2007). All of these problems need to be overcome before the approach can be routinely applied to solar data.

A variety of numerical solution methods have been proposed for the nonlinear force-free equations, including current-field iteration (*e.g.*, Grad and Rubin, 1958; Sakurai, 1981; Amari, Boulmezaoud, and Mikic, 1999; Wheatland, 2006), magnetofrictional methods (*e.g.*, Chodura and Schlueter, 1981; Valori, Kliem, and Keppens, 2005), direct vertical integration of the equations (*e.g.*, Wu *et al.*, 1990), the optimization approach (Wheatland, Sturrock, and Roumeliotis, 2000; Wiegelmann, 2004), and the boundary element method (Yan and Sakurai, 2000). Many of the methods are slow and may be too inefficient to be applied to new, high-resolution boundary data (Schrijver *et al.*, 2006). For three-dimensional problems on grids with N^3 points, the speed of a method may be described by the scaling of the time taken as a function of N. Recently, Wheatland (2006) presented a nonlinear method based on the current-field iteration approach (Grad and Rubin, 1958) that scales as N^4, making it one of the fastest approaches (see also Inhester and Wiegelmann, 2006). Work on understanding and improving nonlinear force-free methods continues (*e.g.*, Amari, Boulmezaoud, and Aly, 2006).

It is important to have appropriate test cases for nonlinear force-free methods. The axisymmetric nonlinear examples of Low and Lou (1990) have been widely used (*e.g.*, Wheatland, Sturrock, and Roumeliotis, 2000; Wiegelmann *et al.*, 2006; Schrijver *et al.*, 2006; Inhester and Wiegelmann, 2006; Amari, Boulmezaoud, and Aly, 2006), but they are limited in that the boundary conditions on α are not very localized. Solar magnetic field measurements provide lower boundary values for the normal component of the field and α over restricted regions on the Sun. Hence appropriate test cases should have all boundary information localized in spatial extent. Titov and Démoulin (1999) constructed a force-free equilibrium consisting of a twisted flux tube embedded in a background potential field, which has localized nonzero α. This example has also been considered as a test case for nonlinear force-free methods (Wiegelmann *et al.*, 2006). However, the Titov – Démoulin equilibrium is also not localized in that the background potential field is produced in part by a (buried) infinite line

current, so the boundary conditions on B_n are not localized. The calculations in Wiegelmann *et al.* (2006) highlighted this limitation in that the Titov – Démoulin equilibrium was not well reproduced by the nonlinear methods using localized lower boundary data.

This paper presents some specific improvements to the Wheatland (2006) method for calculation of nonlinear force-free fields. In particular a new method of solving the Poisson equation in three dimensions using 2-D Fourier transforms is exploited. This solution is analogous to the Fourier solution to the linear force-free equations commonly used in the solar context (Nakagawa and Raadu, 1972; Alissandrakis, 1981). This paper also presents the application of the improved nonlinear force-free code to a class of linear force-free fields that have $B_n = 0$ everywhere except in localized spots. For these fields the boundary conditions on both B_n and $J_n = \alpha B_n/\mu_0$ for the nonlinear method are localized, so they are well suited to testing nonlinear force-free methods. This point does not appear to have been noticed in the literature before.

The layout of the paper is as follows. The improvements to the nonlinear force-free method are outlined in Section 2. The application to linear force-free test cases is given in Section 3, and conclusions are presented in Section 4.

2. Improvements to Method

2.1. Current-Field Iteration

Wheatland (2006) presented a fast version of current-field iteration (Grad and Rubin, 1958), and a variety of implementations of current-field iteration have been proposed (*e.g.*, Sakurai, 1981; Amari, Boulmezaoud, and Mikic, 1999; Inhester and Wiegelmann, 2006). The general approach in a half space $z > 0$ (where $z = 0$ is the boundary) involves solution, at iteration k, of the linear equations

$$\nabla \times \mathbf{B}^{k+1} = \alpha^k \mathbf{B}^k \tag{3}$$

and

$$\left(\mathbf{B}^{k+1} \cdot \nabla\right)\alpha^{k+1} = 0 \tag{4}$$

subject to the boundary conditions

$$\hat{\mathbf{z}} \cdot \mathbf{B}^{k+1}\big|_{z=0} = \hat{\mathbf{z}} \cdot \mathbf{B}^{\text{obs}}\big|_{z=0} \tag{5}$$

and

$$\alpha^{k+1}(x, y, 0)\big|_{B_z>0} = \alpha^{\text{obs}}(x, y, 0)\big|_{B_z>0}, \tag{6}$$

where α^{obs} and $\mathbf{B}^{\text{obs}}$ denote given boundary values and $\hat{\mathbf{z}}$ is the unit vector in the z direction. Alternatively, the last boundary condition may be replaced by

$$\alpha^{k+1}(x, y, 0)\big|_{B_z<0} = \alpha^{\text{obs}}(x, y, 0)\big|_{B_z<0}; \tag{7}$$

that is, boundary values of α^{obs} on the negative polarity may be used. The iteration is generally started with $\mathbf{B}^0$ chosen to be the potential field matching the boundary conditions on the right-hand side of Equation (5).

2.2. Wheatland (2006) implementation

The Wheatland (2006) implementation solves Equation (3) as follows. The field in $z > 0$ is separated into potential and nonpotential components: $\mathbf{B}^{k+1} = \mathbf{B}_0 + \mathbf{B}_{\rm c}^{k+1}$, with the potential component $\mathbf{B}_0$ satisfying

$$\nabla \times \mathbf{B}_0 = 0 \tag{8}$$

and

$$\hat{\mathbf{z}} \cdot \mathbf{B}_0\big|_{z=0} = \hat{\mathbf{z}} \cdot \mathbf{B}^{\rm obs}\big|_{z=0}. \tag{9}$$

The potential field is calculated initially by using a Fourier solution (Alissandrakis, 1981). The nonpotential component $\mathbf{B}_{\rm c}$ satisfies

$$\nabla \times \mathbf{B}_{\rm c}^{k+1} = \alpha^k \mathbf{B}^k \tag{10}$$

in $z > 0$, subject to

$$\hat{\mathbf{z}} \cdot \mathbf{B}_{\rm c}^{k+1}\big|_{z=0} = 0. \tag{11}$$

Equation (10) is recast as Poisson's equation by introducing the vector potential $\mathbf{B}_{\rm c}^{k+1} = \nabla \times \mathbf{A}_{\rm c}^{k+1}$, and adopting the Coulomb gauge ($\nabla \cdot \mathbf{A}_{\rm c}^{k+1} = 0$). The current distribution in all space is assumed to be

$$\mathbf{J}_{\rm c}^k = \begin{cases} \alpha^k \mathbf{B}^k / \mu_0 & \text{for } z \geq 0, \\ \left[-J_{{\rm c}x}^k(x, y, -z), -J_{{\rm c}y}^k(x, y, -z), J_{{\rm c}z}^k(x, y, -z) \right] & \text{for } z < 0. \end{cases} \tag{12}$$

Poisson's equation

$$\nabla^2 \mathbf{A}_{\rm c}^{k+1} = -\mu_0 \mathbf{J}_{\rm c}^k \tag{13}$$

is then solved using 3-D Fourier transforms. The symmetry of the current distribution (12) ensures the boundary condition (11) in the plane $z = 0$.

These steps solve Equation (3). To solve Equation (4), field line tracing is used. For each point $\mathbf{r}$ on the computational grid, the field line threading the point is traced in both directions. If the field line leaves the box by the side or top boundaries of the grid, then $\alpha(\mathbf{r})$ is assigned to be zero. If the field line connects to $z = 0$ at both ends, $\alpha(\mathbf{r})$ is assigned equal to the value of α at the positive polarity end of the field line (or, alternatively, the negative polarity end may be used). The prescription that field lines that leave the grid by the side or top boundaries carry no current provides a simple way to deal with the problem of missing boundary information on $z = 0$ outside of the region at the base of the computational grid. Other approaches are also possible, and we will return to this question in Section 4.

Convergence of the method may be determined by monitoring the change in the current-weighted average angle between the current density and the magnetic field at each iteration (Wheatland, Sturrock, and Roumeliotis, 2000), or the change in the magnetic energy at each iteration.

The time taken to solve Equation (3) scales as $N^3 \log N$, and the time taken to solve Equation (4) scales as N^4. The number of iterations is not dependent (or is only very weakly dependent) on N. The overall time taken then scales with the slowest step (*i.e.* as N^4). Because of this relatively fast scaling, the method may be applied to larger grids. For example, in a recent workshop (Metcalf *et al.*, 2007), the code was applied to test cases on a $320 \times 320 \times 256$ grid.

2.3. Modifications

The method of solution of Equation (3) just described is simple and fast, but it has a drawback. To calculate a field on an $N_x \times N_y \times N_z$ grid, the current density $\mathbf{J}_c^k$ is constructed on a grid with size $N_x \times N_y \times 2N_z$. The doubling of the vertical dimension is undesirable when large grids are used, because of the memory use involved in storing the arrays associated with the calculation. The problem is exacerbated if the arrays are enlarged by padding with zeroes in all three dimensions. In the code described in Wheatland (2006) the arrays are padded to the nearest power of two in all three dimensions, so that the size of the grid involved in the Fourier transform solution is $2^{\text{ceiling}(\log_2 N_x)} \times 2^{\text{ceiling}(\log_2 N_y)} \times 2^{\text{ceiling}(\log_2 2N_z)}$. The padding with zeroes is not strictly required; it is done to reduce the appearance of periodicity introduced by discrete Fourier transforms, and to permit the use of simple fast Fourier transform (FFT) routines. Provided the current density is localized near the center of the computational grid, the padding makes little difference. As an example, for the tests performed on a $320 \times 320 \times 256$ grid described in Metcalf *et al.* (2007), the arrays used in the Fourier transform solution have size $512 \times 512 \times 512$. A vector field represented in single precision on a grid this size requires 1.5 GB of memory. In the following we describe a method of solution of Equation (3) that does not require doubling the vertical dimension of the arrays and hence has smaller memory requirements.

We consider solution of Poisson's equation

$$\nabla^2 \mathbf{A}_c^{k+1} = \alpha^k \mathbf{B}^k \tag{14}$$

in the half space $z > 0$. Hereafter we write $-\mu_0 \mathbf{J}^k$ to represent the right-hand side of this equation. The boundary condition (11) is satisfied if we choose

$$A_{cx}^{k+1}\big|_{z=0} = A_{cy}^{k+1}\big|_{z=0} = 0, \tag{15}$$

and the gauge condition implies the additional boundary condition

$$\left.\frac{\partial A_{cz}^{k+1}}{\partial z}\right|_{z=0} = 0. \tag{16}$$

We also require the boundary conditions $\mathbf{A}_c^{k+1} \to 0$ as $z \to \infty$.

Equation (14) may be solved subject to the stated boundary conditions by Fourier transforming in x and y. The transformed equation is

$$\frac{d^2 \widetilde{\mathbf{A}}_c^{k+1}}{dz^2} - \kappa \widetilde{\mathbf{A}}_c^{k+1} = -\mu_0 \widetilde{\mathbf{J}}^k, \tag{17}$$

where $\widetilde{\mathbf{A}}_c^{k+1} = \widetilde{\mathbf{A}}_c^{k+1}(u, v, z)$, $\widetilde{\mathbf{J}}^k = \widetilde{\mathbf{J}}^k(u, v, z)$, and $\kappa = 4\pi^2(u^2 + v^2)$, with u and v representing wave numbers. The Fourier-transformed boundary conditions are

$$\widetilde{A}_{ci}^{k+1}\big|_{z=0} = 0 \quad \text{for } i = x, y, \tag{18}$$

$$\left.\frac{d\widetilde{A}_{cz}^{k+1}}{dz}\right|_{z=0} = 0, \tag{19}$$

and

$$\widetilde{\mathbf{A}}_c^{k+1} \to 0 \quad \text{as } z \to \infty. \tag{20}$$

Equation (17) is a linear, nonhomogeneous, second-order ODE, and the general solution may be represented in terms of the sum of the two independent solutions of the homogeneous ODE and a particular solution of the nonhomogeneous ODE (*e.g.*, Arfken and Weber, 2001). This general solution contains six constants of integration, which may be determined by imposing the boundary conditions (18) – (20). The resulting solutions for the Fourier-transformed vector potential are

$$\widetilde{A}_{ci}^{k+1} = \frac{\mu_0}{2\kappa}\left(I_{1i} + I_{2i} - I_{3i}\right), \tag{21}$$

for $i = x, y$, and

$$\widetilde{A}_{cz}^{k+1} = \frac{\mu_0}{2\kappa}\left(I_{1z} + I_{2z} + I_{3z}\right), \tag{22}$$

where

$$I_{1i} = \int_z^\infty \mathrm{e}^{-\kappa(s-z)}\,\widetilde{J}_i^k(u, v, s)\,\mathrm{d}s, \tag{23}$$

$$I_{2i} = \int_0^z \mathrm{e}^{-\kappa(z-s)}\,\widetilde{J}_i^k(u, v, s)\,\mathrm{d}s, \tag{24}$$

and

$$I_{3i} = \int_0^\infty \mathrm{e}^{-\kappa(z+s)}\,\widetilde{J}_i^k(u, v, s)\,\mathrm{d}s. \tag{25}$$

We note that Equations (21) and (22) could be written in somewhat simpler forms using $\sinh(\kappa z)$, etc. However, from a computational point of view the stated forms are preferable in that each of the integrals (23) – (25) explicitly approaches zero as $z \to \infty$. Alternative forms require numerical cancellation of large terms as $z \to \infty$.

The Fourier transform of the field $\mathbf{B}_c^{k+1}$ may be obtained from Equations (21) – (25) by using the Fourier transform of $\mathbf{B}_c^{k+1} = \nabla \times \mathbf{A}_c^{k+1}$. The results may be written as

$$\widetilde{B}_{cx}^{k+1} = -\frac{\mu_0}{2\kappa}\left[2\pi \mathrm{i} v(I_{1z} + I_{2z} + I_{3z}) + \kappa(I_{1y} - I_{2y} + I_{3y})\right], \tag{26}$$

$$\widetilde{B}_{cy}^{k+1} = \frac{\mu_0}{2\kappa}\left[\kappa(I_{1x} - I_{2x} + I_{3x}) + 2\pi \mathrm{i} u(I_{1z} + I_{2z} + I_{3z})\right], \tag{27}$$

and

$$\widetilde{B}_{cz}^{k+1} = \frac{\mu_0}{2\kappa}\left[-2\pi \mathrm{i} u(I_{1y} + I_{2y} - I_{3y}) + 2\pi \mathrm{i} v(I_{1x} + I_{2x} - I_{3x})\right]. \tag{28}$$

The computational procedure is as follows. The current density $\mathbf{J}^k = \alpha^k \mathbf{B}^k/\mu_0$ is calculated on an $N_x \times N_y \times N_z$ grid. The arrays are then padded with zeroes in the x and y directions to the nearest power of two (*i.e.,* the grid size is $2^{\mathrm{ceiling}(\log_2 N_x)} \times 2^{\mathrm{ceiling}(\log_2 N_y)} \times N_z$). The padding is again not essential, but it reduces the appearance of periodicity in the solution and permits the use of simple FFT routines. The padded current density arrays are then numerically 2-D Fourier transformed (in x and y) at each value of z, and Equations (26) – (28) are used to construct the 2-D Fourier transform of $\mathbf{B}_c^{k+1}$ at each z. The integrals (23) – (25) are performed by using the extended trapezoidal rule. Because of the method of construction of $\alpha(\mathbf{r})$ the current density is zero above some height in the box, and hence the integrals (23) and (25) are performed to this height rather than to the upper limit of infinity. The results are then numerically inverse Fourier transformed at each z to yield $\mathbf{B}_c^{k+1}$.

The new method of solution of Poisson's equation has a different scaling for the time taken. The time-limiting step is that, at each point on the grid, integrals in one dimension need to be performed. The integrals require of order N operations for each of N^3 points, so this step scales as N^4. Hence the new method of solution of Equation (3) has the same scaling as the solution of Equation (4), and overall the method is expected to scale as N^4. Numerical experiments confirm this expectation, so the new method has the same overall scaling as the previous approach. The advantage of the new method is that it requires only half as much storage space for the arrays holding values of the current density and the vector potential. This is expected to provide a substantial advantage when the method is applied to high -resolution data.

A number of other modifications of the method described in Wheatland (2006) have also been implemented. Some of these are simple changes to improve the efficiency of the code. For example, in the solution of Equation (4) the field line tracing is started from grid points in the plane $z = 0$ and progresses upward through the grid. The code now identifies (at each iteration) the minimum height $z_{\min}$ at which $\alpha(x, y, z_{\min}) = 0$ for all x and y. This is the maximum height of field lines that connect to $z = 0$ at both ends. The values of $\alpha(x, y, z)$ for $z > z_{\min}$ are then immediately set to zero, without further field line tracing. The value $z_{\min}$ is also used as the upper limit in the integrals (23) and (25), as mentioned previously.

A further modification concerns the choice of the boundary conditions on α. As already stated, there is a choice in the assignment of $\alpha(\mathbf{r})$ between the value α_+ at the positive polarity end of the field line threading the point $\mathbf{r}$ and the value α_- at the negative polarity end. This may be used to safeguard against inconsistent boundary values of α, as suggested by Inhester and Wiegelmann (2006). Those authors suggest using a weighted average of α_+ and α_-, the weights depending on the relative reliabilities of the boundary values. We consider instead the equally weighted average $\alpha(\mathbf{r}) = \frac{1}{2}(\alpha_+ + \alpha_-)$. For simple (consistent) test cases such as the Low and Lou (1990) fields, we find that this choice gives comparable results to the choices $\alpha_\pm$.

In common with the Wheatland (2006) code, the new code is parallelized by using OpenMP (*e.g.*, Chandra *et al.*, 2002), for use on shared memory parallel computers. The method is also well suited to parallelization for distributed memory architectures, *e.g.*, using MPI (*e.g.*, Gropp, Lusk, and Skjellum, 1999), as discussed in Section 4.

3. Demonstration on Linear Force-Free Test Cases

The modified method has been tested on the cases considered in Wheatland (2006) and found to give very similar results. This is as expected, since the method differs only in the treatment of the vertical boundary conditions. In this section we consider the application to a different problem, a class of linear force-free fields, to illustrate both the utility of these test cases and the method.

3.1. Linear Force-Free Test Cases

We consider linear force-free fields with $B_n = 0$ except in restricted patches. Linear force-free fields have α constant in space, in which case the force-free equations reduce to the Helmholtz equation, which has well-known solutions (*e.g.*, Nakagawa and Raadu, 1972; Alissandrakis, 1981). Choosing $B_n = 0$ except in local patches has the advantage that the boundary conditions for application of the nonlinear methods (*e.g.*, B_n together with the value of α where $B_n > 0$) are localized.

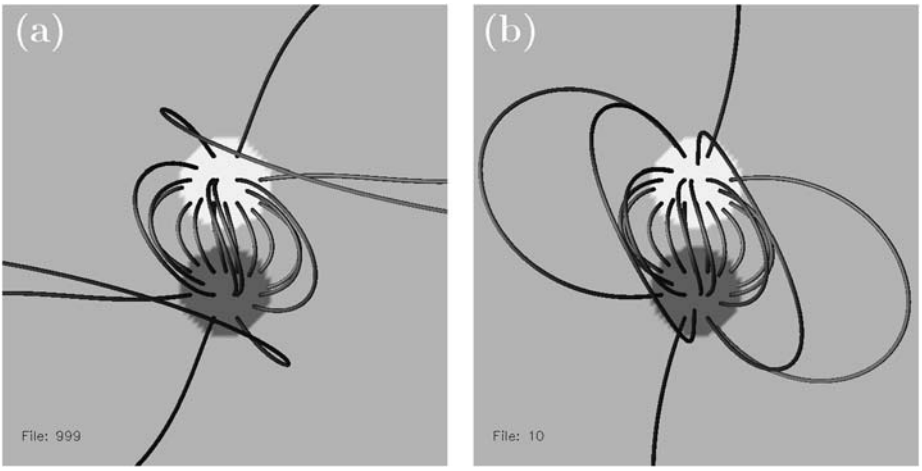

Figure 1 Test Case 1: (a) The linear force-free field. (b) The nonlinear force-free reconstruction.

As a specific example we consider a bipole consisting of two circular pillboxes in the boundary $0 \le x \le L$, $0 \le y \le L$:

$$B_{\rm n}(x,y) = \begin{cases} B_0 & \text{if } (x-\frac{1}{2}L)^2 + (y-\frac{1}{2}L+R)^2 \le a^2, \\ -B_0 & \text{if } (x-\frac{1}{2}L)^2 + (y-\frac{1}{2}L-R)^2 \le a^2\,, \\ 0 & \text{otherwise.} \end{cases} \tag{29}$$

To keep the bipole relatively localized we choose $a = 0.05L$ and $R = 0.06L$ (referred to as Case 1). We also need to choose a value of α. A solution with finite energy exists provided the Fourier components of the boundary conditions on $B_{\rm n}$ are zero for wave numbers u and v such that $(u^2+v^2)^{1/2} \le |\alpha|/(2\pi)$ (Alissandrakis, 1981). This solution is known as the small-scale solution. We assume the boundary conditions are represented on an $M \times M$ grid over the region $0 \le x \le w$, $0 \le y \le w$ with $w \ge L$, the greater extent being padded with zeroes. The smallest nonzero wave numbers associated with discrete Fourier transforms of the boundary conditions then have magnitude $u_{\rm min} = v_{\rm min} = 1/(M\Delta x)$, where Δx is the spatial step. (The Fourier component for $u = v = 0$ is zero because the flux is balanced.) This implies the limit $\alpha \le 2\pi/(M\Delta x)$ for the small-scale solutions. In the following we consider calculations on a $200 \times 200 \times 200$ grid, so there are $N = 200$ points between $x = 0$ and $x = L$, and $\Delta x = L/(N-1)$. For the Fourier transform solution of Poisson's equation we pad with zeroes in the x and y directions to size $M = 256$. In that case the limit is $\alpha L \le 2\pi(N-1)/M \approx 4.88$. We consider $\alpha L = 4.85$, very close to the maximum value.

The results for Case 1 are shown in Figure 1. Panel (a) in the figure shows the linear force-free test case calculated using the small scale solution (Alissandrakis, 1981). The view is looking down on the central part of the computational domain from above. The boundary values of $B_{\rm n}$ are shown as a gray-scale image in the lower boundary, and some representative field lines are shown as tubes. Panel (b) in the figure shows the nonlinear force-free field obtained with the current-field iteration method after 10 iterations. The method converges rapidly, and at the tenth iteration the fractional change in the energy is $\approx 10^{-6}$. The calculation (on a $200 \times 200 \times 200$ grid) took approximately two hours using four processor cores, and the peak memory use was 600 MB. The view in panel (b) is the same as in panel (a), and in particular field lines are drawn from the same starting points. There is good agreement for the low-lying field lines linking the two poles, but the higher field lines disagree.

Table 1 Measures of agreement between the linear force-free test case and the nonlinear reconstruction.

Field	C_{vec}	C_{CS}	E'_{n}	E'_{m}	ϵ
Case 1	0.999	0.956	0.901	0.729	0.994
Case 2	1.000	1.000	0.985	0.972	1.000

This disagreement occurs because points $\mathbf{r}$ on the computational grid threaded by field lines that leave the grid by the side or top boundaries have $\alpha(\mathbf{r}) = 0$, according to the procedure described in Section 2.2. Hence there is an absence of current in "open-field" regions, by comparison with the linear force-free solution. This difference means that the nonlinear calculation will never exactly reproduce the linear force-free solution. This point illustrates the handling of the boundary conditions on current in the present method.

To quantify the agreement (and disagreement) between the linear force-free solution and the nonlinear reconstruction in Case 1, we consider the metrics presented in Schrijver *et al.* (2006), namely the vector correlation (C_{vec}), the Cauchy – Schwarz correlation (C_{CS}), the complement of the normalized vector error (E'_{n}), the complement of the mean vector error (E'_{m}), and the relative magnetic energy (ϵ). These quantities should all be unity for a perfect reconstruction. For a solution field $\mathbf{B}_i$ and a reconstructed field $\mathbf{b}_i$ defined at S points the metrics are

$$C_{\mathrm{vec}} = \frac{\sum_{i=1}^{S} \mathbf{B}_i \cdot \mathbf{b}_i}{(\sum_{i=1}^{S} |\mathbf{B}_i|^2)^{1/2} (\sum_{i=1}^{S} |\mathbf{b}_i|^2)^{1/2}}, \tag{30}$$

$$C_{\mathrm{CS}} = \frac{1}{S} \sum_{i=1}^{S} \frac{\mathbf{B}_i \cdot \mathbf{b}_i}{|\mathbf{B}_i||\mathbf{b}_i|}, \tag{31}$$

$$E'_{\mathrm{n}} = 1 - \frac{\sum_{i=1}^{S} |\mathbf{B}_i - \mathbf{b}_i|}{\sum_{i=1}^{S} |\mathbf{B}_i|}, \tag{32}$$

$$E'_{\mathrm{m}} = 1 - \frac{1}{S} \sum_{i=1}^{S} \frac{|\mathbf{B}_i - \mathbf{b}_i|}{|\mathbf{B}_i|}, \tag{33}$$

and

$$\epsilon = \frac{\sum_{i=1}^{S} \mathbf{b}_i \cdot \mathbf{b}_i}{\sum_{i=1}^{S} \mathbf{B}_i \cdot \mathbf{B}_i}. \tag{34}$$

The first row of Table 1 presents the stated metrics for Case 1 calculated for the inner one-third of the computational grid, which just encompasses the boundary location of the poles (indices 67:122, 67:122, and 0:65, in the x, y, and z directions). There is reasonable agreement, although the discrepancy is clear, in particular for the metrics E'_{n} and E'_{m}.

We also consider a second case (Case 2) in which the bipole is reduced in size by half ($a = 0.025L$ and $R = 0.03L$), for the same value of α ($\alpha = 4.85$) and the same grid size ($200 \times 200 \times 200$). In this case the bipole is more localized, so we expect a better reproduction using the nonlinear force-free method. Figure 2 shows the boundary conditions and field lines for Case 2, in the same presentation as Figure 1 (in particular the field of view is the same). Once again the field lines close to the bipole are accurately reproduced, but the field lines further from the bipole are less well reproduced. The second row of Table 1 also presents metrics for Case 2. In this example the metrics are calculated for the inner

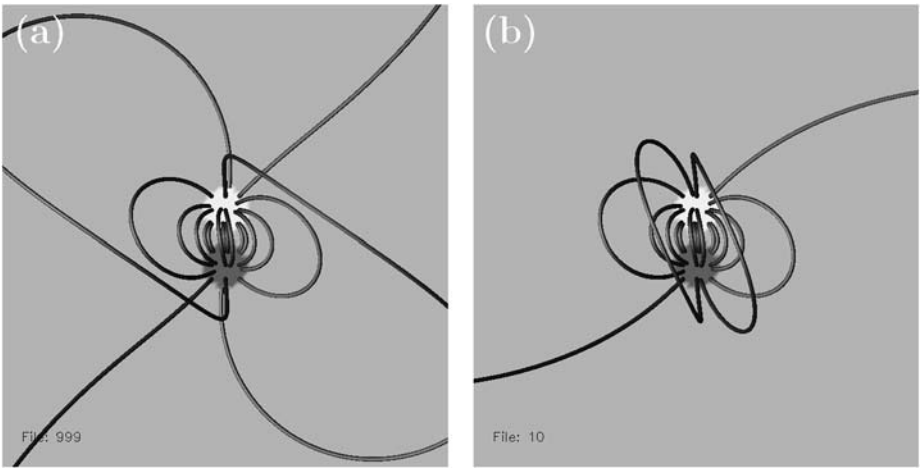

Figure 2 Test Case 2: (a) The linear force-free field. (b) The nonlinear force-free reconstruction.

one-sixth of the grid (indices 84:115, 84:115, and 0:31, in x, y and z, respectively), which is the appropriate subsection of the grid for comparison with Case 1. The metrics are significantly improved compared to Case 1 because a smaller fraction of field lines originating at the poles leave the computational grid by the side or top boundaries.

4. Conclusions

This paper presents improvements to a method for calculating nonlinear force-free fields (Wheatland, 2006). The modified approach uses a novel solution to Poisson's equation in three dimensions using 2-D Fourier transforms (Section 2.3). The advantage of this approach, rather than the original approach using 3-D Fourier transforms, is that the arrays holding the field values are halved in size. This permits the method to be applied to larger grids, which is important given the advent of high-resolution vector magnetic field data from new solar observing instruments, including the Solar Optical Telescope on *Hinode* (Shimizu, 2004) and the upcoming Helioseismic and Magnetic Imager on the *Solar Dynamics Observatory*. The method of solution of Poisson's equation is analogous to the method of solution of the Helmholtz equation commonly used to calculate linear force-free fields (*e.g.*, Nakagawa and Raadu, 1972; Alissandrakis, 1981).

The new method is demonstrated in application to linear force-free test cases with isolated patches of nonzero B_n, the normal component of the field in the boundary. The boundary conditions for nonlinear calculations are B_n together with the force-free parameter α specified over the region with $B_n > 0$ (or the region where $B_n < 0$). Hence our test cases have localized boundary conditions on both B_n and $J_n = \alpha B_n/\mu_0$, and so they are suitable test cases for nonlinear force-free methods. In particular the method is applied to a bipole pillbox configuration. The nonlinear method provides an approximate reconstruction of the test field. It does not perfectly reproduce the field because points $\mathbf{r}$ on the computational grid threaded by field lines that leave the grid via the side or top boundaries are assigned $\alpha(\mathbf{r}) = 0$. In this way the nonlinear force-free method addresses the problem of the missing information associated with the boundary conditions on field and current outside of the specified boundary region. This example highlights a general problem: All nonlinear force-free

methods (and indeed potential and linear force-free methods) must make some assumptions and approximations to deal with missing boundary information.

The procedure of assigning $\alpha(\mathbf{r}) = 0$ at points threaded by field lines that leave the side or top of the grid is not the only possible way to deal with the problem of missing boundary information. For example, another self-consistent procedure (*i.e.,* one ensuring $\nabla \cdot \mathbf{J} = 0$) would be to assume $\alpha(\mathbf{r})$ is spatially periodic in x and y with period corresponding to the lengths of the sides of the padded boundary region used in the Fourier solutions. In principle this would permit $\alpha(\mathbf{r})$ to be determined for points threaded by field lines that connect at only one end to the lower boundary by extending the field line tracing to allow crossing of the boundaries. This would permit a more accurate reconstruction in the case of the linear force-free solutions considered in Section 3, because the test case solutions are themselves periodic. [The test case solutions are the Alissandrakis (1981) discrete Fourier solutions.] However, the exact solution would not be reproduced even in these cases because some field lines do not connect to the lower boundary at either end. We do not pursue this idea, because in general it assumes an artificial periodicity, and it is not clear to what extent it would be useful for reconstructions based on real solar data. We consider the present handling of assignment of $\alpha(\mathbf{r})$ to be an appropriate, simple solution to the problem of the "missing information" presented by field lines that connect outside of the boundary region in the solar reconstruction problem. We note that it does not imply restrictions of balanced flux or current in application to real magnetograms. Real magnetograms may have current-carrying field lines that leave the region for which boundary values are available: we are simply ignoring that current, because to model it accurately requires information that is unavailable.

The present method is a promising candidate for modeling coronal magnetic fields from spectropolarimetrically derived solar boundary data, in particular because of its speed. [In common with the Wheatland (2006) method, the time taken scales as N^4 for a calculation on a grid with N^3 points, making it at least as fast as any other method.] However, high-resolution data will still require long computation times, and parallelization is desirable. The code used here is parallelized using OpenMP, for use on shared memory parallel computers (Chandra *et al.*, 2002). The method is also well suited to parallelization for distributed memory architectures, *e.g.*, using MPI (Gropp, Lusk, and Skjellum, 1999). The two steps in current-field iteration – solution of Equation (3) and solution of Equation (4) – may both be parallelized in simple ways. Specifically, in solving Equation (3) the 2-D Fourier transforms for different values of z on the grid may be performed in parallel, and in solving Equation (4), the field line tracing from different points on the grid may be performed in parallel. These approaches may be implemented using either OpenMP or MPI. In future an MPI version of the code will be written, to permit large-scale parallelization.

In a recent test of nonlinear force-free methods on a solar-like test case (Metcalf *et al.*, 2007), the two best performing methods were the present method and the optimization method (Wheatland, Sturrock, and Roumeliotis, 2000; Wiegelmann, 2004). The two methods appear to have various advantages and disadvantages. Optimization is comparably fast, and in particular it has been implemented with an N^4 scaling for computation time (Inhester and Wiegelmann, 2006). A possible advantage of the present method is that the optimization method uses all three components of the vector field in the boundary, in which case the boundary value problem is not well posed (Amari, Boulmezaoud, and Aly, 2006). This problem is not important for test cases with consistent boundary data, but it is likely to be important in application to real data. However, the "preprocessing" procedure appears to go some way toward solving this problem (Wiegelmann, Inhester, and Sakurai, 2006; Metcalf *et al.*, 2007), and conversely it may be argued that the present method relies on accurate determination of boundary values of α, which is difficult with present data. A possible

advantage of the present method is that it may be applied to cases for which vector magnetic field values are available over only one polarity (provided B_n is available on the other polarity). In general it may be said that the application to solar boundary data is a difficult problem and the utility of methods is hard to anticipate without actual numerical experimentation. It will also be hard to assess the success of reconstructions. In this regard the ability to choose between the positive polarity and negative polarity of the boundary field for the specification of $\alpha(\mathbf{r})$ may be seen as an additional advantage of the present method, in that it allows a simple test of the dependence of the reconstruction on the choice of boundary conditions on current.

Acknowledgements The author thanks Dr Boris Kuhlmey for a careful reading of the manuscript and an anonymous referee for a detailed and constructive report.

References

Alissandrakis, C.E.: 1981, *Astron. Astrophys.* **100**, 197.
Arfken, G.B., Weber, H.J.: 2001, *Mathematical Methods for Physicists*, Harcourt Academic Press, San Diego.
Amari, T., Boulmezaoud, T.Z., Aly, J.J.: 2006, *Astron. Astrophys.* **446**, 691.
Amari, T., Boulmezaoud, T.Z., Mikic, Z.: 1999, *Astron. Astrophys.* **350**, 1051.
Amari, T., Aly, J.J., Luciani, J.F., Boulmezaoud, T.Z., Mikic, Z.: 1997, *Solar Phys.* **174**, 129.
Chandra, R., Dagum, L., Kohr, D., Maydan, D., McDonald, J., Menon, R.: 2002, *Parallel Programming in OpenMP*, Morgan Kaufmann, San Francisco.
Chodura, R., Schlueter, A.: 1981, *J. Comput. Phys.* **41**, 68.
Grad, H., Rubin, H.: 1958, In: *Proc. 2nd Int. Conf. on Peaceful Uses of Atomic Energy* **31**, United Nations, Geneva, 190.
Gropp, W., Lusk, E., Skjellum, A.: 1999, *Using MPI: Portable Parallel Programming with the Message-Passing Interface*, 2nd edn., MIT Press, Cambridge.
Inhester, B., Wiegelmann, T.: 2006, *Solar Phys.* **235**, 201.
Low, B.C., Lou, Y.Q.: 1990, *Astrophys. J.* **352**, 343.
McClymont, A.N., Jiao, L., Mikic, Z.: 1997, *Solar Phys.* **174**, 191.
Metcalf, T.R., Jiao, L., McClymont, A.N., Canfield, R.C., Uitenbroek, H.: 1995, *Astrophys. J.* **439**, 474.
Metcalf, T.R., Leka, K.D., Barnes, G., Lites, B.W., Georgoulis, M.K., Pevtsov, A.A., *et al.*: 2006, *Solar Phys.* **237**, 267.
Metcalf, T.R., DeRosa, M.L., Schrijver, C.J., Barnes, G., van Ballegooijen, A., Wiegelmann, T., Wheatland, M.S., Valori, G., McTiernan, J.: 2007, *Solar Phys.*, submitted.
Nakagawa, Y., Raadu, M.A.: 1972, *Solar Phys.* **25**, 127.
Neukirch, T.: 2005, In: Innes, D.E., Lagg, A., Solanki, S.K. (eds.) *Proceedings of the International Scientific Conference on Chromospheric and Coronal Magnetic Fields, ESA SP 596*, 12.1 (CD-ROM).
Sakurai, T.: 1981, *Solar Phys.* **69**, 343.
Schrijver, C.J., Derosa, M.L., Metcalf, T.R., Liu, Y., McTiernan, J., Régnier, S., Valori, G., Wheatland, M.S., Wiegelmann, T.: 2006, *Solar Phys.* **235**, 161.
Shimizu, T.: 2004, In: Sakurai, T., Sekii, T. (eds.) *The Solar-B Mission and the Forefront of Solar Physics, Astron. Soc. Pacific Conf. Ser.* **325**, 3.
Titov, V.S., Démoulin, P.: 1999, *Astron. Astrophys.* **351**, 707.
Valori, G., Kliem, B., Keppens, R.: 2005, *Astron. Astrophys.* **433**, 335.
Wheatland, M.S.: 2006, *Solar Phys.* **238**, 29.
Wheatland, M.S., Sturrock, P.A., Roumeliotis, G.: 2000, *Astrophys. J.* **540**, 1150.
Wiegelmann, T.: 2004, *Solar Phys.* **219**, 87.
Wiegelmann, T., Inhester, B., Sakurai, T.: 2006, *Solar Phys.* **233**, 215.
Wiegelmann, T., Inhester, B., Kliem, B., Valori, G., Neukirch, T.: 2006, *Astron. Astrophys.* **453**, 737.
Wu, S.T., Sun, M.T., Chang, H.M., Hagyard, M.J., Gary, G.A.: 1990, *Astrophys. J.* **362**, 698.
Yan, Y., Sakurai, T.: 2000, *Solar Phys.* **195**, 89.